# Measuring cosmic defect correlations in liquid crystals

Rajarshi Ray*
*Tata Institute of Fundamental Research, Mumbai, 400005, India*

Ajit M. Srivastava†
*Institute of Physics, Sachivalaya Marg, Bhubaneswar 751005, India*

(Received 11 December 2001; revised manuscript received 10 December 2003; published 28 May 2004)

From the theory of topological defect formation proposed for the early Universe, the so-called Kibble mechanism, it follows that the density correlation functions of defects and antidefects in a given system should be completely determined in terms of a single length scale $\xi$, the relevant domain size, which is proportional to the average interdefect separation $r_{av}$. Thus, when lengths are expressed in units of $r_{av}$, these distributions should show universal behavior, depending only on the symmetry of the order parameter and space dimensions. We have verified this prediction by analyzing the distributions of defects and antidefects formed during the isotropic-nematic phase transition in a thin layer in a liquid crystal sample. Our experimental results confirm this prediction and are in reasonable agreement with the results of numerical simulations.

DOI: 10.1103/PhysRevD.69.103525 PACS number(s): 98.80.Cq, 61.30.Jf, 64.70.Md

## I. INTRODUCTION

The big-bang theory of the Universe is well established by now, with most of the observations being in good agreement with the predictions of the model. Accurate measurements of the cosmic microwave background radiation (CMBR) have made cosmology into a precision science where competing models of the early Universe are put to rigorous tests. One of the models which was very popular earlier for explaining the formation of structure in the Universe, such as galaxies, clusters, and superclusters of galaxies, utilized the concept of *topological defects*, in particular cosmic string defects [1]. However, recent CMBR anisotropy data are not in agreement with predictions of topological-defect-based models of structure formation. Data are in very good agreement with the predictions of density fluctuations from inflation, though at present it cannot be ruled out that defects may also contribute to some part of structure formation [2] (see, also, Ref. [3]). Further, topological defects arise in many particle physics models of the unification of forces, and their presence in the early Universe can lead to other important consequences, such as the production of baryon numbers below the electroweak scale, generating baryon number inhomogeneities at the quark-hadron transition, etc. [4]. It is therefore important to deepen our understanding of how these defects form in the Universe [5] and how they evolve. This paper relates to the first of these issues.

There are numerous examples of topological defects in condensed matter systems, such as flux tubes in superconductors, vortices in superfluid helium, monopoles and strings in liquid crystals, etc. It has long been known that such defects routinely form during a phase transition. The first detailed theory of the formation of topological defects in a phase transition (apart from the usual equilibrium process of thermal production) was proposed by Kibble [6,7] in the context of the early Universe. It is usually referred to as the *Kibble mechanism*. It was first suggested by Zurek [8] that some of the aspects of the Kibble mechanism can be tested in condensed matter systems, such as superfluid $^4$He. Indeed the basic physical picture of the Kibble mechanism applies equally well to a condensed matter system [9,10,5,11]. Using this correspondence, the basic picture of defect formation was first observed by Chuang *et al.* in an isotropic to nematic (I-N) transition in liquid crystal systems [12]. The formation and evolution of string defects was observed to be remarkably similar to what had been predicted for the case of the Universe, apart from obvious differences such as the velocity of defects, time scales of the evolution of the defect network, etc. Subsequently, measurements of the string density were carried out by observing strings formed in the first-order I-N transition occurring via the nucleation of nematic bubbles in the isotropic background [13]. The results were found to be in good agreement with the prediction of the Kibble mechanism. (For testing the Kibble mechanism in other condensed matter systems, see Refs. [14,15].) Yet another quantitative measurement was made of the exponent characterizing the correlation between the defects and antidefects formed in the I-N transition in liquid crystals, with results in good agreement with the Kibble mechanism [16].

It is certainly dramatic that there is a correspondence between the phenomena expected to have occurred in the early Universe, during stages when its temperature was about $10^{29}$ K, with those occurring in condensed matter systems at temperatures less than a few hundred K. The important question is whether the observations and measurements performed in condensed matter systems provide rigorous tests of the theories being used to predict phenomena in the early Universe, or they simply provide an analogy with the case of the early Universe or, at best, examples of other systems where *similar theoretical considerations* can be made for investigating defect formation. On the face of it, the differences between the two cases seem so profound that a rigorous test of the theories underlying the phenomena taking place in the early Universe seems out of question within the

*Email address: rajarshi@theory.tifr.res.in
†Email address: ajit@iopb.res.in

 

domain of condensed matter systems. For example, a description of the matter, transformations between its various phases, etc., in the early Universe is given in terms of elementary particle physics models, which require the framework of relativistic quantum field theory. Indeed, typical velocities of particles, and even of topological defects formed in such transitions, are close to the velocity of light. On the other hand, in condensed matter systems nonrelativistic quantum mechanics provides an adequate description of most relevant systems. Typical velocities in such systems are extremely small in comparison. For example, in liquid crystals, the typical velocity of string defects is of the order of a few microns per second, completely negligible in comparison to the speed of light. Similarly, the value of the string tension (i.e., string energy per unit length) for the case of the Universe is of the order of $10^{32}$ GeV$^2$ (in natural units) which is about $10^{18}$ tons/cm. In contrast, in condensed matter systems (say, in liquid crystals), the string tension is governed by the scale of the free energy of the order of $10^{-2}$ eV (e.g., the free energy of a liquid crystal string of length about the coherence length will be of this order). Indeed, it is due to this extremely large string tension (i.e., mass per unit length) of cosmic string defects that they were proposed to have seeded formation of galaxies, clusters of galaxies, etc., via their gravitational effects. Clearly such effects are unthinkable for string defects in liquid crystals or in superfluid helium, etc.

Despite the fact that the two systems look completely dissimilar, it turns out that there are ways in which specific condensed matter experiments can provide rigorous tests of the theories of cosmic defect formation. This can be done by identifying those predictions of the theory which show universal behavior. As we will discuss below there are several predictions of the Kibble mechanism which show universal behavior when expressed in terms of a suitable length scale.

The paper is organized in the following manner. In Sec. II, we review the basic picture of defect formation. The correlations of defects and antidefects are discussed in Sec. III. Section IV describes the numerical simulation and expected behavior of density correlation functions of defects. The experiment is described in Sec. V, while experimental results and simulation results are discussed in Sec. VI. Conclusions are presented in Sec. VII.

## II. PHYSICAL PICTURE OF DEFECT FORMATION

We first recall the basic physics of the Kibble mechanism [6,7,10]. For concreteness, we consider the case of a complex scalar order parameter $\phi$, with spontaneously broken U(1) symmetry (as in the case of the Abelian Higgs model, superconductors, or superfluid $^4$He). The order parameter space (the vacuum manifold) is a circle $S^1$ in this case. Here, string (vortex) defects arise when the phase $\theta$ of $\phi$ winds nontrivially around the order parameter space $S^1$. (Later we will see that in our present experiment also, where defects form at the I-N interface, the anchoring of the order parameter at the I-N interface leads to the effective order parameter space being $S^1$, rather than the usual $RP^2$ for nematic liquid crystals.) In the Kibble mechanism, defects form due to a domain structure arising in a phase transition. This domainlike structure arises from the fact that during the phase transition, the phase $\theta$ of the order parameter field $\phi$ can only be correlated within a finite region. $\theta$ can be taken to be roughly uniform within a region (domain) of size $\sim\xi$, while varying randomly from one domain to the other. This situation is very natural to expect in a first-order phase transition where the transition to the spontaneous symmetry-broken phase happens via nucleation of bubbles. Inside a bubble, $\theta$ will be uniform, while $\theta$ will vary randomly from one bubble to another. Eventually bubbles grow and coalesce, giving rise to a region of space where $\theta$ varies randomly at a distance scale of the interbubble separation, thereby leading to a domainlike structure. [In certain situations—e.g., when the bubble wall motion is highly dissipative—the effective domain size may be larger [17,5]. In between any two adjacent bubbles (domains), $\theta$ is supposed to vary with the least gradient. This is usually called the *geodesic rule* and arises naturally from consideration of minimizing the gradient energy for the case of global symmetry. For gauge symmetry, the situation is more complicated, though it has been shown that under certain situations the geodesic rule continues to hold [18]. However, the geodesic rule may not hold in the presence of strong fluctuations [19–21]. See, also, Ref. [22] in this context. Recently it has been shown [21] that a defect distribution very different from what is expected in the Kibble mechanism may arise when defect formation is dominated by magnetic field fluctuations.]

The same situation happens for a second-order transition where the orientation of the order parameter field is correlated only within a region of the size of the correlation length $\xi$. This again results in a domainlike structure, with domains being the correlation volumes. We mention that there are nontrivial issues in the case of a second-order phase transition in determining the appropriate correlation length for calculating the *absolute initial defect density*, where the appropriate value of $\xi$ may depend on the rate of the phase transition [7] (see, also, [5]). It was shown by Zurek [9] that the appropriate value of $\xi$ should be determined by incorporating the effects of the critical slowing down of the dynamics of the order parameter field near the transition temperature. The theory which takes into account this (for second-order transitions) is usually referred to as the *Kibble-Zurek* mechanism. Here, the absolute defect density is determined by critical fluctuations of the order parameter and depends on details such as the rate of cooling of the system, etc. For a discussion of these issues, see Ref. [9]. We emphasize that these considerations of the details of the critical dynamics of the order parameter field during the phase transition are important in calculating the absolute defect density. However, the defect density *per domain* is insensitive to these details.

For the U(1) case which we are discussing, string defects (vortices) arise at the junctions of domains if $\theta$ winds nontrivially around a closed path going through adjacent domains. Consider a junction $P$ of three domains, as shown in Fig. 1. For simplicity, we show here domains as spheres (e.g., bubbles for a first-order transition), with the centers of the three nearest bubbles forming an equilateral triangle. The values of $\theta$ in these three domains are $\theta_1$, $\theta_2$, and $\theta_3$. One

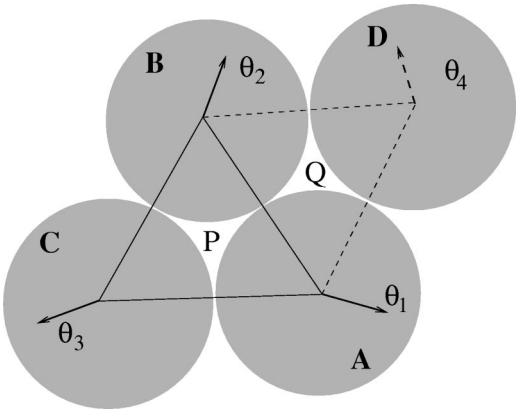


FIG. 1. Defect formation due to coalescence of three domains.

can show that with the use of the geodesic rule (i.e., the variation of $\theta$ in between any two domains is along the shortest path on the order parameter space $S^1$), a nontrivial winding of $\theta$ (i.e., by $\pm 2\pi$) along a closed path, encircling the junction $P$ and going through the three domains $A$, $B$, $C$, will arise only when $\theta_3$ lies in the (shorter) arc between $\theta_1+\pi$ and $\theta_2+\pi$. The maximum and minimum values of the angular span of this arc are $\pi$ and 0, with the average angular span being $\pi/2$. Since $\theta_3$ can lie anywhere in the circle, the probability that it lies in the required range is $p=(\pi/2)/(2\pi)=1/4$. Thus, we conclude [23] that the probability of vortex (or antivortex) formation at a junction of three domains (in two space dimensions) is equal to 1/4.

It is important to realize that in the above argument, no use is made of the field equations. Thus, whether the system is a relativistic one for particle physics or a nonrelativistic one appropriate for condensed matter physics, there is no difference in the defect production per domain. (This is so as long as the geodesic rule holds. As we have mentioned above, this may not be true when the field dynamics is dominated by fluctuations [19–21]. In those situations, defect production will be determined by some different processes—e.g., by a new *flipping mechanism* [19,20] or by fluctuating magnetic fields [21], again, apart from the usual equilibrium thermal production.) Therefore, the expected number of defects *per domain* has universal behavior, in the sense that it only depends on the symmetry of the order parameter and the space dimensions. It is this universal nature of the prediction of defect density (number of defects per domain) in the Kibble mechanism because of which the measurements of defects per domain in liquid crystals in Ref. [13] provide a rigorous test of the Kibble mechanism (which was originally given for cosmic defect production). Note that the absolute defect density does not show universal behavior since it depends on the domain size $\xi$. The entire dependence on the dynamical details of the specific system is through the single length scale $\xi$. Thus, when densities are expressed in the length scale of $\xi$ the prediction acquires a universal character.

### III. DEFECT-ANTIDEFECT CORRELATIONS

The Kibble mechanism not only predicts the number density of defects. It also predicts a very specific correlation between the defects and antidefects. Again, by focusing on specific quantities and choosing proper length scales, this prediction acquires a universal nature which can then be tested experimentally in condensed matter systems. This prediction is important as in many experimental situations it can provide the only rigorous test of the underlying theory of defect formation. This is for the following reason. As we have discussed above, the prediction of defect density becomes universal only when expressed in the length units of the domain size. For a first-order transition it can be done easily if the average bubble diameter (assuming small variance in bubble sizes) can be experimentally determined, as in the liquid crystal experiments in Ref. [13]. However, this is a highly nontrivial problem for the case of second-order transitions or for spinodal decomposition. For experimental situations with a second-order transition (type-II superconductors, superfluid $^4$He), it has not been possible to make an independent determination of the correlation length relevant for defect formation. All one can do is to measure the absolute defect density, comparison of which to the prediction from theory becomes dependent on various details of the phase transition, which determine the relevant correlation length [9].

Defect-antidefect correlations, on the other hand, imply specific spatial distributions of defects, which are independent of the prediction of the defect density. Within the framework of the Kibble mechanism, defect density distributions are expected to reflect defect-antidefect correlations at the typical distance scales of a domain size. At the same time, the typical interdefect separation $r_{av}$, as given by $\rho^{-1/2}$ where $\rho$ is the average defect-antidefect density, is directly proportional to the domain size $\xi$. From this, one can conclude that if defect and antidefect distributions are expressed in terms of the average interdefect separation $r_{av}$, then these should display universal behavior, the important point being that the same experiment yields the value of the average interdefect separation ($r_{av}=\rho^{-1/2}$), and the defect and antidefect distributions are analyzed by using this length scale. Details such as the bubble size or the relevant correlation length, therefore, become completely immaterial for testing the predictions regarding correlations.

To understand how this correlation between defects and antidefects arises, let us go back to Fig. 1. With the directions of arrows shown there (which denote values of $\theta$), we see that a defect (vortex with winding $+1$) has formed at $P$. Let us address the issue that, given that a defect has formed at $P$, how does the probability of a defect, or antidefect, change in the nearest triangular region—say, at $Q$. At $Q$, the three domains which intersect are $A$, $B$, and $D$. Here $\theta$ already has a specific variation in $A$ and $B$ in order to yield a defect at $P$. From the point of view of $Q$, this variation in $A$ and $B$ is a partial winding configuration for an antivortex. With partial antiwinding present in $A$ and $B$, it can be seen from Fig. 1 that whatever the value of $\theta$ in $D$, it is impossible to have a vortex at $Q$ (i.e., $\theta$ winding by $+2\pi$ as we go around $Q$ in an anticlockwise manner). On the other hand, the probability of an antivortex formation at $Q$ is 1/4 by straightforward repetition of the argument given above to calculate the probability of the formation of a vortex *or* antivortex at a junction

of three domains. This is the most dramatic example of the correlation between defect and antidefect formation. If we consider defect formation due to the intersection of (say) four domains, this correlation still exists; that is, close to a defect, the formation of another defect is less likely (though not completely prohibited now) and the formation of an antidefect is enhanced. This conclusion about a certain correlation in the formation of a defect and an antidefect is valid for other types of defects as well [24,25]. (See, for example, Ref. [24] for a discussion of the correlation between global monopoles and antimonopoles.)

To see what this correlation implies, let us consider a two-dimensional region $\Omega$ whose area is $A$ and whose perimeter $L$ goes through $L/\xi$ number of elementary domains (where $\xi$ is the domain size). As $\theta$ varies randomly from one domain to another, one is essentially dealing with a random walk problem with the average step size for $\theta$ being $\pi/2$ (the largest step is $\pi$ and the smallest is zero). Thus, the net winding number of $\theta$ around $L$ will be distributed about zero with a typical width given by $\sigma=\frac{1}{4}\sqrt{L/\xi}$, implying that $\sigma \propto A^{1/4}$ (see Refs. [26,16,10]). Assuming roughly uniform defect density, we get $\sigma \propto N^{1/4}$ (where $N$ is the total number of defects in the region $\Omega$), which reflects the correlation in the production of defects and antidefects. In the absence of any correlations, the net defect number will not be as suppressed and will follow a Poisson distribution with $\sigma \sim \sqrt{N}$. In general one may write the following scaling relation for $\sigma$:

$$\sigma = CN^{\nu}. \tag{1}$$

The exponent $\nu$ will be 1/2 for the uncorrelated case and 1/4 for the case of the Kibble mechanism. Again, the prediction of $\nu=1/4$ is of universal nature, depending only on the symmetry of the order parameter and space dimensions. An experimental measurement of this exponent was carried out in Ref. [16]. The experimental value of $\nu$ was found in Ref. [16] to be $\nu=0.26\pm0.11$ which is in good agreement with the predicted value of 1/4 from the Kibble mechanism and reflects the correlated nature of defects and antidefects.

The exponent $\nu$ does not give complete information about the correlation which arises between defects and antidefects when they are produced via the Kibble mechanism. A more detailed understanding of the correlation can be achieved by calculating the density correlation function of the defects and antidefects. Below, we first discuss the theoretical prediction about this and then describe the experimental measurements.

## IV. NUMERICAL SIMULATION

We have carried out the numerical simulation of defect formation via the Kibble mechanism for the square lattice case (instead of the triangular case as shown in Fig. 1) where defects will form at the intersection of four domains; see Fig. 2. This is because we find slightly better agreement with the experimental results for the square lattice case. We will also quote results for the triangular lattice case. The probability $p$ of a defect or an antidefect per square region (in Fig. 2) is obtained to be 0.33. We start with the origin $O$ of the coordinate system to be at the center of a square containing a

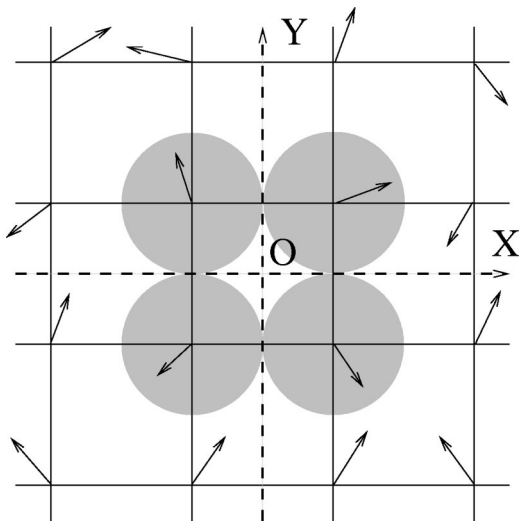


FIG. 2. Defect formation due to the coalescence of four elementary domains, forming a square lattice.

defect (making sure that $O$ is at least one domain away from the boundary). We then calculate the density of antidefects, $\rho_{\bar{d}}(r)$, as well as the density of defects, $\rho_d(r)$, as a function of the radial distance $r$ from the defect at the origin. For this, we count number of antidefects (defects) in an annular region of width $\Delta r$ centered at distance $r$ from the origin and divide this number by the area of the annular region. An average of these densities (for a given $r$) is taken by taking different defects at the origin, as well as by taking many realizations of the event of defect production. With the density in the central square (which has a defect) appropriately normalized, this is the same as the density correlation function of defects. As should be clear by now, all dynamical details of the specific model are relevant only in determining the domain size $\xi$ (i.e., either the bubble diameter for a first-order transition case or the relevant correlation length for a second-order transition case or for spinodal decomposition). For the simulation, we take domain size to be unity, meaning that all lengths are measured in units of domain size. All remaining properties of the defect distributions should now display universal behavior, depending only on the symmetry of the order parameter [U(1) in this case], space dimensions (2 here), and, possibly, fundamental domain structure (square versus triangular). Another important factor here is that there is no reason to expect that the defect or antidefect will be exactly at the center of the square formed by the centers of the four bubbles (domains). In realistic situations, the defects can be anywhere in the elementary square, which in some sense represents the collision region of the four correlation domains (bubbles). However, since the correlation domains, by definition, have uniform order parameter, it should be increasingly unlikely that the defect is far from the center of the collision region (i.e., away from $O$). To take into account of these physical considerations, we have allowed the position of defects and antidefects to float within a square with an approximately Gaussian probability distribution, centered in the middle of the square, with varying width. By changing the width of this distribution we can change from almost-

centered defects to defects with uniform probability in the elementary square region.

With this picture and with a defect being in the central square, we know that the probability of antidefect formation should be enhanced in the nearest squares, while the probability of defect formation should be suppressed in these regions. These defects and antidefects cannot be too close to the central defect as that would imply variation of the order parameter at distance scales much smaller than $\xi$. One therefore expects that both $\rho_{\bar{d}}(r)$ and $\rho_d(r)$ will be almost zero for $r \ll \xi$ (discounting the central defect at $O$). Both densities will rise as $r$ increases. At a distance of about $r \sim \xi$, one expects a peak in $\rho_{\bar{d}}(r)$. The height of this peak will determine the suppression in $\rho_d(r)$ (compared to the asymptotic value) at that point.

For $r \geqslant 2\xi$ one expects both distributions to approach the average density expected asymptotically. This conclusion may appear surprising as one might have expected that increased antidefect probability in the nearest square may imply suppressed antidefect probability in the next-nearest square, etc., leading to a damped oscillatory behavior of $\rho_{\bar{d}}(r)$ and $\rho_d(r)$ (similar to the density correlation function for a liquid). The reason that this does not happen here is simple and, again, intrinsic to the Kibble mechanism. Recall that the antidefects were enhanced (and defects suppressed) in the squares nearest to the central square because, for each of these four squares, two out of four vertices had $\theta$ common to the central square which already had a defect. The probability of defects and antidefects in these squares was, therefore, affected by the presence of defects in the central square. In contrast, $\theta$ at three vertices of the *next-nearest* (corner) squares and at all vertices farther away are completely random. This implies that the probability of defects and antidefects must be equal in all such regions, leading to a flattening of $\rho_{\bar{d}}(r)$ and $\rho_d(r)$ for $r \geqslant 2\xi$. As we will see below, this theoretical reasoning is well borne out by the results of the simulations and is consistent with the experimental results, within error bars.

We have explained above that this analysis of defect-antidefect correlations does not require knowledge of the domain size. In fact, the power of this technique is best illustrated in those experimental situations where domains are not identifiable (as in the experiments explained below). The length scale $\xi$ is, therefore, not a convenient choice from this point of view. We instead will use the interdefect separation $r_{av}$ to define our length scale. If the probability of defect formation per (square) domain is $p$, then $r_{av}$ and $\xi$ are related in the following manner:

$$r_{av} = \frac{\xi}{\sqrt{p}}. \tag{2}$$

In our experiment, we have tried to record the defect distributions immediately after their formation. Occasionally, some evolution of the defect network occurs by a coarsening of domains. This makes the effective correlation domain size $\xi$ larger, so the above relation still holds. Coarsening of domains only makes the effective correlation domain size $\xi$ larger. Since the probability $p$ (defects per domain) is also of universal nature, it follows from Eq. (2) that the distributions $\rho_{\bar{d}}(r)$ and $\rho_d(r)$ will still show universal behavior if $r$ is measured in units of $r_{av}$. As $r_{av}$ can be directly measured for a given defect distribution, without any recourse to the underlying domain structure, we will use it as defining the unit of length. In this unit, the peak in $\rho_{\bar{d}}(r)$ will be expected to occur at $r = \sqrt{p} \simeq 0.57$ with $p = 0.33$ for the square lattice case. (This is when the order parameter space is $S^1$, which, as we will discuss below, is the case for our experiment.) By $r = 2\sqrt{p} \simeq 1.14$, both densities will be expected to flatten out to the asymptotic value of 0.5. The asymptotic value of $\rho_d$ and $\rho_{\bar{d}}$ is 0.5 since by definition the unit length $r_{av}$ is the average separation between defects and antidefects. The height of the peak for $\rho_{\bar{d}}$ (at $r \simeq 0.57$) depends on the weight factor for centering the defects and antidefects inside square regions. This is simply because perfectly centered defects and antidefects will lead to large contributions when the centers of the squares fall inside the annular regions for calculating densities, while for neighboring values of $r$, their contributions will be zero. When defects and antidefect positions are floated, then the contributions are averaged out. We find that the height of the peak varies from about 1.2 for perfectly centered defects and antidefects to about 0.75 for the case when defects and antidefect positions are uniformly distributed inside a square. When comparing with the experimental results, we choose the weight factor appropriately so that the height of the peak in $\rho_{\bar{d}}$ from simulations is similar to the one obtained from experiments. (It will be interesting to investigate the physics contained in the peak height resulting from this weight factor for centering the defects in a square, which may depend on the interactions between defects and antidefects.)

If we take the thickness of the annular region $\Delta r$ (for calculating densities) to be about the domain size (i.e., 0.57 in units of $r_{av}$), then one can relate the suppression in $\rho_d$ at $r = \sqrt{p} \simeq 0.57$ to the height of the peak in $\rho_{\bar{d}}$ at that position. This is done as follows. Note that the values of $\theta$ at all the outer 12 vertices of the 8 squares, bordering the central square containing the defect, are completely random (i.e., they are not constrained by the fact that there is a defect in the central square). Let us consider the distribution of the net winding along the large square-shaped closed path going through all these 12 vertices. Repetition of the earlier argument [in writing Eq. (1)] shows that this net winding should be distributed about the value zero (and should have a typical width proportional to $\sqrt{12}$, but this part is not relevant here). Thus, the average number of defects $n_d$ inside this large square should be same as the average number of antidefects, $n_{\bar{d}}$.

Out of these eight outer squares, there are four squares, each of which share one edge (i.e., two vertices) with the central square containing the defect. As a result of the presence of the defect in the central square, there will be a partial winding present at this edge (on average), affecting the probabilities of defects and antidefects in these four outer squares. We take the densities for these squares to be given by $\rho_d(r = 0.57)$, and $\rho_{\bar{d}}(r = 0.57)$ for defects and antidefects,

respectively. Now the remaining four squares (out of the outer eight squares) are at the corners and share only one vertex with the central square containing the defect. Clearly, the presence of defects in the central square cannot have any effect on the probabilities of defects or antidefects in these corner squares. (Also, these corner squares are at a distance which is farther away from the center than $r=0.57$.) We denote the defect density (or the antidefect density, both being equal for these squares) as $\rho_0$.

Now, using the fact that the central square always has one defect and that the area of each domain is $\xi^2=p$ in the units of $r_{av}$, we can write down the condition that on average the defect number should equal the antidefect number in the area containing all nine squares (including the central one):

$$1+4p\rho_d(r=0.57)+4p\rho_0=4p\rho_{\bar{d}}(r=0.57)+4p\rho_0. \quad (3)$$

This leads to the following relation between $\rho_d$ and $\rho_{\bar{d}}$ at $r\simeq 0.57$:

$$\rho_d(r=0.57)=\rho_{\bar{d}}(r=0.57)-\frac{1}{4p}\simeq\rho_{\bar{d}}(r=0.57)-0.76, \quad (4)$$

for $p=0.33$.

As we will see later, our simulation results as well as experimental data are in reasonable agreement with this crude estimate.

## V. EXPERIMENT

Our experiments have been carried out using nematic liquid crystals. For uniaxial nematic liquid crystals (NLCs) the orientation of the order parameter in the nematic phase is given by a unit vector (with identical opposite directions) called the director. The order parameter space is $RP^2$ $(\equiv S^2/Z_2)$, which allows for string defects with strength-1/2 windings. As a result of the birefringence of NLCs, when the liquid crystal sample is placed between crossed polarizers, then in regions where the director is either parallel or perpendicular to the electric field $\vec{E}$, the polarization is maintained, resulting in a dark brush. At other regions, the polarization changes through the sample, resulting in a bright region. This implies that for a defect of strength $s$, one will observe $4s$ dark brushes [27]. If the cross-polarizer setup is rotated, then brushes will rotate in the same (opposite) direction for positive (negative) windings. Equivalently, if the sample is rotated between fixed crossed polarizers, then brushes do not rotate for $+1$ winding while they rotate in the same direction (with twice the angle of rotation of the sample) for $-1$ winding. We have used this method to determine the windings. (For earlier studies of the director field orientations as well as defects in liquid crystals see, e.g., [28].)

We now describe our experiment. We observed the I-N transition in a tiny droplet (size $\sim 2-3$ mm) of NLC 4′-pentyl-4-biphenyl-carbonitrile (98% pure, purchased from Aldrich Chem.). The sample was placed on a clean, untreated glass slide and was heated using an ordinary lamp. The I-N transition temperature is about 35.3 °C. Our setup allowed the possibility of slow heating and cooling by changing the distance of the lamp from the sample. We observed the defect production very close to the transition temperature (in some cases we had some isotropic bubbles coexisting with the nematic layer containing defects). For the observations, we used a Leica, DMRM microscope with $20\times$ objective, a charge-coupled-device (CCD) camera, and a cross-polarizer setup, at the Institute of Physics, Bhubaneswar. The phase transition process was recorded on a standard video cassette recorder. The images were photographed directly from a television monitor by replaying the cassette.

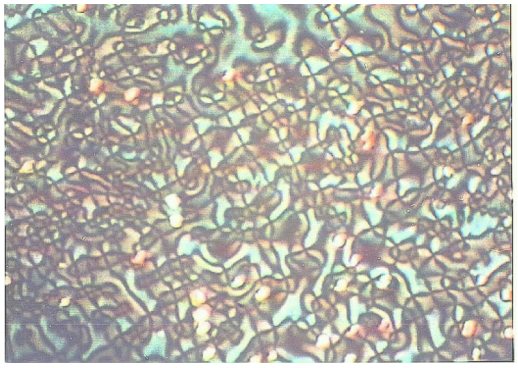

FIG. 3. Network of strength-1 defects and antidefects formed in the I-N transition. Crossing of brushes denotes defects with winding $\pm 1$. Size of the image is about 0.45 mm$\times$0.32 mm.

The I-N transition is of first order. When the transition proceeds via nucleation of bubbles, we observe long horizontal strings (as in Ref. [13]), which are not suitable for our present analysis. We selected those events where the transition seems to occur uniformly in a thin layer near the top of the droplet (possibly due to faster cooling from contact with air). The depth of field of our microscope was about 20 $\mu$m. All defects in the field of view were well focused, suggesting that they formed in a thin layer, especially since typical interdefect separation was about 10–40 $\mu$m. (For us, the only thing relevant is that the layer be effectively two dimensional over distances of the order of a typical interdefect separation.) Also, the transition happened over the entire observation region roughly uniformly, suggesting that a process like spinodal decomposition may have been responsible for the transition. This resulted in a distribution of strength-($\pm 1$) defects as shown in the photograph in Fig. 3. Points from which four dark brushes emanate correspond to defects of strength $\pm 1$. As a result of the resolution limitation the crossings here do not appear as point like. It is practically impossible to use the technique of the rotation of brushes to identify every winding in situations such as shown in Fig. 3 due to the very small interdefect separation (resulting from a high defect density), as well as due to the rapid evolution of the defect distribution.

We have developed a particular technique for determining the individual windings of defects in situations like Fig. 3 where one only needs to determine the winding of one of the defects by rotation in a cross-polarizer setup. The windings of the rest of the defects can then be determined using topological arguments; see Ref. [16] for details of this technique.

Further, as explained in Ref. [16], the anchoring of the director at the I-N interface in our experiment forces the director to lie on a cone, with half angle equal to about 64° (see Ref. [29]). This forces the order parameter space there to become effectively a circle $S^1$, instead of being $RP^2$, with the order parameter being an angle between 0 and $2\pi$. The only defects allowed now are ones with integer windings, which is consistent with the fact that no strength-1/2 defects are seen in our experiment [16]. Therefore the predictions of the Kibble mechanism for the U(1) case, as described above, are valid for this case, with the picture that a domain structure near the I-N interface is responsible for the formation of integer windings (see Ref. [16] for a detailed discussion of these points).

## VI. RESULTS AND DISCUSSION

After identifying the windings of all defects (wherever possible) in a picture, we note the positions ($x$-$y$ coordinates) of each defect and antidefect in the picture. We then determine the average defect-antidefect density $\rho$. With the average interdefect separation $r_{av}$ being $\rho^{-1/2}$, we convert all coordinate distances into scaled distances by dividing by $r_{av}$. We then choose one defect as the origin, making sure that the defect is at least 1 unit (with the unit length being $r_{av}$ now) away from the boundary of the picture. The density of defects, $\rho_d(r)$, as well as the density of antidefects, $\rho_{\bar{d}}(r)$, is now calculated for each $r$ (at a step size of $\Delta r$) by counting number of defects (antidefects) within an annular region of thickness $\Delta r$ centered at $r$. Different values of $\Delta r$ are used to get the least possible statistical fluctuations, while at the same time retaining the structure of the peak, etc. The same $\Delta r$ is used in numerical simulations for comparison with the experimental data. We will present the results for $\Delta r = 0.25$ (in the units of $r_{av}$). The calculation is repeated by taking other defects as origins, and an average of densities (for a given value of $r$) is taken to determine the final values of $\rho_d(r)$ and $\rho_{\bar{d}}(r)$. To increase the statistics, an average of the distributions is taken by combining the results of all pictures. Different pictures have very different values of $r_{av}$, ranging from about 5 $\mu$m to about 50 $\mu$m. However, when expressed in units of $r_{av}$, the densities $\rho_d$ and $\rho_{\bar{d}}$ show similar behavior for all pictures (at least those ones which had significant statistics). In all, we have analyzed 17 pictures, with the total number of defects and antidefects being 833.

Figure 4 shows the results. The solid plots show the spline fitting of the simulation results which are denoted by open circles. (We mention that statistical errors are very small for the simulation; we have taken a very large number of defects. However, there are larger errors due to uncertainties like the floating of defect positions inside each domain, instead of exact centralization of defects, as explained above in Sec. IV.) We have used a square lattice (shown in Fig. 2) for the simulation, as described above. The antidefect distribution clearly shows a peak near $r \simeq 0.6$ as expected from the Kibble mechanism. The defect density is suppressed in that region at $r \simeq 0.6$, with the simulation results roughly in agreement with the expected suppression—i.e., $\rho_d \simeq \rho_{\bar{d}} - 0.76 \simeq 0.14$ [with $p \simeq 0.33$ and $\rho_{\bar{d}}(r=0.57) \simeq 0.9$]. As expected, both densities reach asymptotic values by $r \sim 1$. The regular oscillations in the densities are due to the regular lattice structure of the simulations, with defects and antidefects remaining close to the centers of the domains. If defects and antidefects are assumed to be strictly at the centers of the domains, then the oscillations in $\rho_{\bar{d}}(r)$ and $\rho_d(r)$ are even more pronounced and regular. At the other extreme, if the positions of defects and antidefects are taken to be uniform within respective domains, then these oscillations completely disappear, except for the prominent peak in $\rho_{\bar{d}}$ at $r \simeq 0.6$. Here we have taken an intermediate case with the positions of defects and antidefects weighted by a Gaussian centered at the middle of the elementary square (so that the peak height is similar to the one obtained from the experiment, as discussed above).

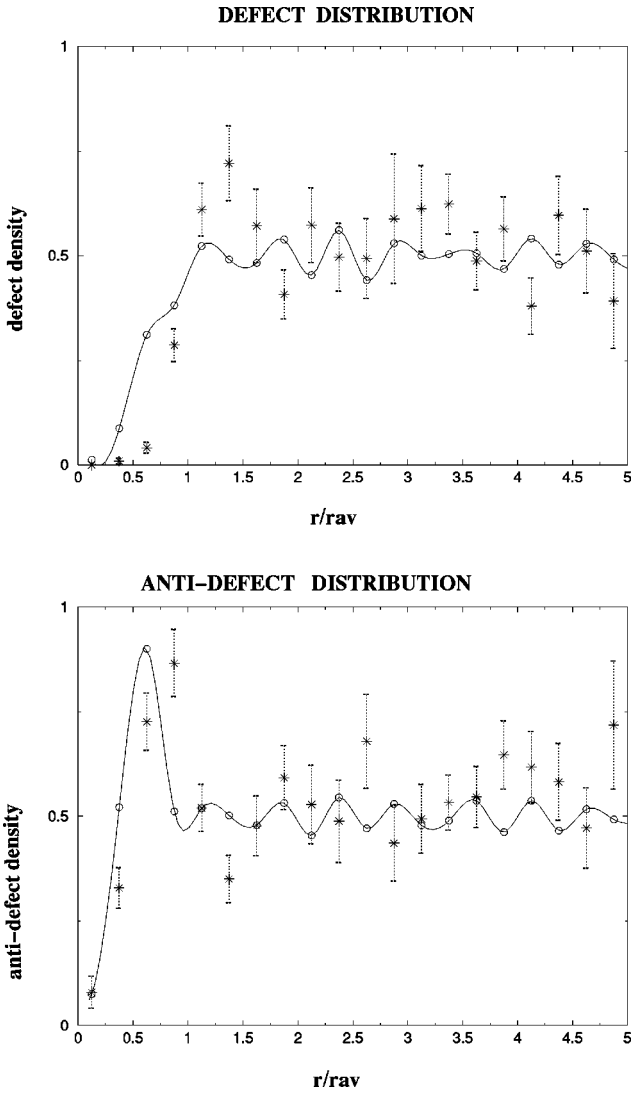


FIG. 4. Solid plots show the simulation results for the defect density $\rho_d(r)$ (top figure) and antidefect density $\rho_{\bar{d}}(r)$ (bottom figure). Stars show the experimental data.

The stars show the experimental values. The error bars have been calculated by taking the error in the count $n$ of defects or antidefects within an annular strip (of the same thickness $\Delta r = 0.25$ used for the simulation) to be $\sqrt{n}$. The

peak in the data points of the antidefect density is prominent and so is the suppression in the defect density for $r<1.0$. The data on the defect density seem to be in reasonably good agreement with the simulation results. Especially the amount of suppression in the defect density for $r\simeq 0.57$ is in good agreement with the crude estimate provided above in Eq. (4). The position of the antidefect peak from experimental data is shifted by about 0.25 on the right, as compared to the peak from the simulation. With the statistics we have at present, it is not possible to resolve whether this shift is genuine or whether it is due to statistical fluctuations. We have done the following checks to address this point. Instead of square elementary domains, if we take triangular domains in the simulation [with due account of geometrical factors in Eq. (2), etc.], we find the simulation peak at about $r\simeq 0.4$—that is, slightly further shifted towards left compared to the experimental peak. This is consistent with the findings in Ref. [16] where it was found that experimental data favored square elementary domains. It is possible that the dynamics of coalescence of domains makes four-domain coalescence more likely than three-domain coalescence. This can be checked by carrying out the simulation of, say, a first-order transition, as in Ref. [30], where one can directly compare the probability of four-bubble coalescence to three-domain coalescence. Again, just as in the case in Ref. [16], the data in the present analysis also do not have enough statistics to make definitive statements about this issue of the preferred shape of elementary domains. Even though it is possible that the simulation peak may shift further to the right for elementary domains with a larger number of sides (which increases the probability $p$), it is clear from Eq. (2) that the position of the peak will always remain at $r<1$ (in units of $r_{av}$).

With a smaller set of data we had seen that the shift between the experimental peak and the simulation peak was larger. With the inclusion of all defects and antidefects (which could be analyzed using our techniques), the shift was reduced, suggesting that it is possible that the shift may be reduced further if larger data are available. Even at present, the shift between the two peaks is relatively small. In fact the shift is about the same as the smallest separation between defects and/or antidefects which we have found in our experiments.

We mention here that defect correlations have been theoretically investigated before [31] and have also been experimentally studied in liquid crystal systems [32]. However, these studies relate to defect correlations for late stages of the evolution of defect networks when the defect network has already entered the scaling regime. This is in contrast to our discussion where defect correlations are investigated at the time of defect formation itself. Depending on the mechanism of defect formation, defect correlations at late stages may be very different from the ones at the time of defect formation. For example, in Ref. [32], density correlation functions of defects and antidefects have been measured and plots similar to those in our paper have been obtained. However, there are very important differences between our work and the experiment reported in Ref. [32]. The most important difference is that in Ref. [32] defect formation was achieved by applying a low-frequency electric field. As discussed in Ref. [32] (see, also, Ref. [33]), this leads to the formation a *bubble* structure such that each bubble contains a defect-antidefect pair [i.e., a $(+1,-1)$ winding pair]. In contrast, in our work defects are produced during a *phase transition* by cooling the sample. As a result of spinodal decomposition, the defect network is formed in a large area. There is *no perfect* correlation between defects and antidefects at the time of formation in our work, while in Ref. [32] every bubble produces a $(+1, -1)$ winding pair. Thus the defect production mechanisms are fundamentally different in the two cases.

Another important difference between our work and that in Ref. [32] is that, as mentioned above, our experiment probes the defect correlations *at the time of defect formation*, the main purpose being to test the Kibble mechanism of the formation of cosmic defects. That is why defects are recorded right at the time of their formation, before any significant defect-antidefect annihilations can take place. In contrast, in Ref. [32], defect correlations are studied during the evolution of the defect network, when the system is already in the scaling regime. In fact it is emphasized in Ref. [32] that the correlation observed arises due to defect-antidefect attraction during the evolution of a defect network. As mentioned above, if defect correlations were studied exactly at the time of formation in Ref. [32], they would have found a perfect correlation between defects and antidefects as each bubble contains a $(+1,-1)$ winding pair. This correlation would then decrease as the defect network evolves by a coarsening of domains. In contrast, in our work there is no perfect correlation between the defects and antidefects at the time of defect formation. (This is why we had to invent a new technique [16] to identify individual windings in dense defect networks as in Fig. 3.) Defect correlations at the time of formation in the Kibble mechanism arise because of the underlying domain picture. As explained above [Eq. (2)], even if defects evolve by a coarsening of domains, this picture remains valid, the only change being an increase of the effective domain size. In contrast, as we discussed above, in the experiment reported in Ref. [32], the defect correlations at the time of formation would be different. However, after defects evolve by coarsening, again a domain picture will emerge. This is why the plots in Ref. [32], which represent defect correlations during the coarsening of domains, look similar to those in our work (which represent defect correlations at the time of formation).

## VII. CONCLUSIONS

The observation of a peak in $\bar{\rho_d}(r)$ (near $r\simeq 0.8$) is roughly in accordance with the theoretical prediction. What is remarkable is that the data show a prominent peak near the position where it is expected and at the same time show a suppression in the defect density by about the right amount, at the same point. At large $r$ there is not sufficient statistics to say whether the densities approach the asymptotic values at $r\simeq 1.1$, though the data are certainly consistent with this in the sense that there are no other prominent peaks visible and the fluctuations are randomly distributed about the asymptotic value. (We note here that it is intriguing that a similar structure of the plots has been seen for the scaled

radial distribution functions of islands formed on a single-crystal substrate [34]. It will be interesting to explore of any possible connection between the two cases.)

We conclude by emphasizing again that our measurements of the density correlation function of defects and antidefects provide a rigorous test of the theory of cosmic defect formation, as well as defect formation in condensed matter systems. For a liquid crystal system, $r_{av}$ is about 10 $\mu$m, while $r_{av}$ will be about $10^{-30}$ cm for cosmic defects (those formed at the grand unified theory transition). However, when expressed in the scaled length $r$ (by dividing by $r_{av}$), one expects in both cases a peak in antidefect density at $r \simeq 0.6$ and a flattening out by $r \simeq 1$ [for the U(1) case and for two-dimensional cross sections of defect networks]. Similarly the defect density is predicted to be suppressed relative to the antidefect density at $r \simeq 0.6$ by a calculable factor, again flattening out by $r \simeq 1$. The experimental data verify both these predictions, though fluctuations due to small statistics are large. It is clearly desirable to be able to carry out an experimental analysis with a significantly larger data set in order to improve the error bars, so that more definitive statements can be made about the comparison between theory and experiments (e.g., about the apparent shift in the peak position). What is very encouraging and remarkable is that by appropriately focusing on the predictions of the theory of cosmic defect formation which acquire universal behavior by a suitable change of length scales, one is able to rigorously test these theories in ordinary condensed matter experiments.

## ACKNOWLEDGMENTS

We are thankful to Mark Srednicki, Shikha Varma, Soma Dey, Sanatan Digal, Soma Sanyal, and Supratim Sengupta for useful discussions. A.M.S. acknowledges the hospitality of the Physics Department, the University of California, Santa Barbara, where one of the early versions of the paper was completed. His work at UCSB was supported by NSF Grant No. PHY-0098395.

[1] A. Vilenkin and E.P.S. Shellard, *Cosmic Strings and Other Topological Defects* (Cambridge University Press, Cambridge, England, 1994); A. Gangui, astro-ph/0110285.

[2] P.P. Avelino and A.R. Liddle, Mon. Not. R. Astron. Soc. **348**, 105 (2004); C. Contaldi, M. Hindmarsh, and J. Magueijo, Phys. Rev. Lett. **82**, 2034 (1999); R.A. Battye and J. Weller, Phys. Rev. D **61**, 043501 (2000); F.R. Bouchet, P. Peter, A. Riazuelo, and M. Sakellariadou, *ibid.* **65**, 021301 (2001).

[3] R. Durrer, astro-ph/0003363; C.R. Contaldi, astro-ph/0005115; L. Pogosian, Int. J. Mod. Phys. A **16**, 1043 (2001); A. Albrecht, astro-ph/0009129.

[4] R.H. Brandenberger, A.C. Davis, and M. Hindmarsh, Phys. Lett. B **263**, 239 (1991); R. Brandenberger, A.C. Davis, and Mark Trodden, *ibid.* **335**, 123 (1994); B. Layek, S. Sanyal, and A.M. Srivastava, Int. J. Mod. Phys. A **18**, 4851 (2003); B. Layek, S. Sanyal, and A.M. Srivastava, Phys. Rev. D **63**, 083512 (2001).

[5] *Formation and Interactions of Topological Defects*, edited by A.C. Davis and R. Brandenberger, Proceedings of NATO Advanced Study Institute (Plenum, New York, 1994); A. Rajantie, hep-ph/0311262; T. Vachaspati, astro-ph/9903362.

[6] T.W.B. Kibble, J. Phys. A **9**, 1387 (1976).

[7] T.W.B. Kibble, Phys. Rep. **67**, 183 (1980).

[8] W.H. Zurek, Nature (London) **317**, 505 (1985).

[9] W.H. Zurek, Phys. Rep. **276**, 177 (1996); P. Laguna and W.H. Zurek, Phys. Rev. Lett. **78**, 2519 (1997); A. Yates and W.H. Zurek, *ibid.* **80**, 5477 (1998); L.M.A. Bettencourt, N.D. Antunes, and W.H. Zurek, Phys. Rev. D **62**, 065005 (2000).

[10] A. Rajantie, Int. J. Mod. Phys. A **17**, 1 (2002).

[11] T.W.B. Kibble, cond-mat/0111082.

[12] I. Chuang, R. Durrer, N. Turok, and B. Yurke, Science **251**, 1336 (1991); R. Snyder *et al.*, Phys. Rev. A **45**, R2169 (1992); I. Chuang *et al.*, Phys. Rev. E **47**, 3343 (1993).

[13] M.J. Bowick, L. Chandar, E.A. Schiff, and A.M. Srivastava, Science **263**, 943 (1994).

[14] P.C. Hendry *et al.*, Nature (London) **368**, 315 (1994); V.M.H. Ruutu *et al.*, *ibid.* **382**, 334 (1996); M.E. Dodd *et al.*, Phys. Rev. Lett. **81**, 3703 (1998); see also G.E. Volovik, Czech. J. Phys. **46**, 3048 (1996).

[15] R. Carmi, E. Polturak, and G. Koren, Phys. Rev. Lett. **84**, 4966 (2000); A. Maniv, E. Polturak, and G. Koren, cond-mat/0304359; R.J. Rivers and A. Swarup, cond-mat/0312082; E. Kavoussanaki, R. Monaco, and R.J. Rivers, Phys. Rev. Lett. **85**, 3452 (2000); S. Rudaz, A.M. Srivastava, and S. Varma, Int. J. Mod. Phys. A **14**, 1591 (1999).

[16] S. Digal, R. Ray, and A.M. Srivastava, Phys. Rev. Lett. **83**, 5030 (1999).

[17] J. Borrill, T.W.B. Kibble, T. Vachaspati, and A. Vilenkin, Phys. Rev. D **52**, 1934 (1995); A. Melfo and L. Perivolaropoulos, *ibid.* **52**, 992 (1995); A. Ferrera and A. Melfo, *ibid.* **53**, 6852 (1996); A. Ferrera, *ibid.* **57**, 7130 (1998).

[18] S. Rudaz and A.M. Srivastava, Mod. Phys. Lett. **A8**, 1443 (1993); R.H. Brandenberger and A.C. Davis, Phys. Lett. B **332**, 305 (1994); T.W.B. Kibble and A. Vilenkin, Phys. Rev. D **52**, 679 (1995).

[19] S. Digal and A.M. Srivastava, Phys. Rev. Lett. **76**, 583 (1996); S. Digal, S. Sengupta, and A.M. Srivastava, Phys. Rev. D **55**, 3824 (1997); **56**, 2035 (1997); **58**, 103510 (1998).

[20] E.J. Copeland and P.M. Saffin, Phys. Rev. D **54**, 6088 (1996).

[21] M. Hindmarsh and A. Rajantie, Phys. Rev. Lett. **85**, 4660 (2000); G.J. Stephens, L.M.A. Bettencourt, and W.H. Zurek, *ibid.* **88**, 137004 (2002).

[22] L. Pogosian and T. Vachaspati, Phys. Lett. B **423**, 45 (1998).

[23] T. Vachaspati, Phys. Rev. D **44**, 3723 (1991).

[24] R. Leese and T. Prokopec, Phys. Lett. B **260**, 27 (1991).

[25] A.M. Srivastava, Phys. Rev. D **43**, 1047 (1991).

[26] T. Vachaspati and A. Vilenkin, Phys. Rev. D **30**, 2036 (1984).

[27] S. Singh, *Liquid Crystals Fundamentals* (World Scientific, River Edge, NJ, 2002); S. Chandrasekhar and G.S. Ranganath, Adv. Phys. **35**, 507 (1986).

[28] D.H. Van Winkle and N.A. Clark, Phys. Rev. A **38**, 1573 (1988); C. Denniston, Phys. Rev. B **54**, 6272 (1996); M. Nakata *et al.*, Phys. Rev. E **64**, 021709 (2001).
[29] S. Faetti and V. Palleschi, Phys. Rev. A **30**, 3241 (1984).
[30] A.M. Srivastava, Phys. Rev. D **46**, 1353 (1992); S. Chakravarty and A.M. Srivastava, Nucl. Phys. **B406**, 795 (1993).
[31] F. Liu and G.F. Mazenko, Phys. Rev. B **46**, 5963 (1992).
[32] T. Nagaya, H. Orihara, and Y. Ishibashi, J. Phys. Soc. Jpn. **64**, 78 (1995).
[33] T. Nagaya, H. Orihara, and Y. Ishibashi, J. Phys. Soc. Jpn. **59**, 377 (1990); T. Nagaya, H. Hotta, H. Orihara, and Y. Ishibashi, *ibid.* **60**, 1572 (1991); **61**, 3511 (1992).
[34] V. Bressler-Hill, S. Varma, A. Lorke, B.Z. Nosho, P.M. Petroff, and W.H. Weinberg, Phys. Rev. Lett. **74**, 3209 (1995).